Journal of Fluids and Structures 44 (2014) 52–66

Contents lists available at ScienceDirect

Journal of Fluids and Structures

journal homepage: www.elsevier.com/locate/jfs

Experimental investigation of the flow-induced vibration of a curved cylinder in convex and concave configurations

Gustavo R.S. Assi [a,*], Narakorn Srinil [b], Cesar M. Freire [c], Ivan Korkischko [c,1]

[a] Department of Naval Architecture and Ocean Engineering, University of São Paulo, São Paulo, Brazil
[b] Department of Naval Architecture and Marine Engineering, University of Strathclyde, Glasgow, UK
[c] Department of Mechanical Engineering, University of São Paulo, São Paulo, Brazil

ARTICLE INFO

Article history:
Received 8 April 2013
Accepted 10 October 2013
Available online 6 November 2013

Keywords:
Vortex-induced vibration
Cross-flow and in-line motion
Curved cylinder
Particle image velocimetry

ABSTRACT

Experiments have been conducted to investigate the two-degree-of-freedom vortex-induced vibration (VIV) response of a rigid section of a curved circular cylinder with low mass-damping ratio. Two curved configurations, a concave and a convex, were tested regarding the direction of the flow, in addition to a straight cylinder that served as reference. Amplitude and frequency responses are presented versus reduced velocity for a Reynolds number range between 750 and 15 000. Results for the curved cylinders with concave and convex configurations revealed significantly lower vibration amplitudes when compared to the typical VIV response of a straight cylinder. However, the concave cylinder showed relatively higher amplitudes than the convex cylinder which were sustained beyond the typical synchronisation region. We believe this distinct behaviour between the convex and the concave configurations is related to the wake interference taking place in the lower half of the curvature due to perturbations generated in the horizontal section when it is positioned upstream. Particle-image velocimetry (PIV) measurements of the separated flow along the cylinder highlight the effect of curvature on vortex formation and excitation revealing a complex fluid–structure interaction mechanism.

1. Introduction

Ongoing deep-sea exploration, installation and production of hydrocarbon energy need the development of new viable technologies. One of these is the requirement of a robust and reliable analysis tool for the prediction of vortex-induced vibration (VIV) of marine structures exposed to ocean currents. Because VIV can cause high cyclic-loading fatigue damage of structures, it is now widely accepted to be a crucial factor that should be taken into account in the preliminary analysis and design. However, many insightful VIV aspects are still unknown and far from fully understood; these render the structural design quite conservative with the use of a large factor of safety. For offshore structures with initial curvatures and high flexibility such as catenary risers, mooring cables and free-spanning pipelines, the theoretical, numerical or experimental VIV research is still very lacking.

* Corresponding author. Current address: PNV Dept. Eng. Naval e Oceanica, Escola Politécnica da Universidade de São Paulo, Av. Prof Mello Moraes 2231, 05508-030, São Paulo - SP, Brazil. Tel.: +55 11 30915646; fax: +55 11 30915642.
E-mail addresses: g.assi@usp.br, gustavo.assi@gmail.com (G.R.S. Assi).
URL: http://www.ndf.poli.usp.br (G.R.S. Assi).
[1] Now at the Institute of Aerodynamics and Flow Technology, German Aerospace Center (DLR), Göttingen, Germany.

0889-9746/$ - see front matter © 2013 Elsevier Ltd. All rights reserved.
http://dx.doi.org/10.1016/j.jfluidstructs.2013.10.011

Nomenclature

D	cylinder external diameter	m^*	mass ratio
f_0	natural frequency in air	Re	Reynolds number
f_x	streamwise oscillation frequency	U	flow speed
f_y	cross-flow oscillation frequency	U/Df_0	reduced velocity
h	cylinder vertical length below the water line	$\hat{x}$	streamwise harmonic amplitude of vibration
		$\hat{y}$	cross-flow harmonic amplitude of vibration
		ζ	structural damping ratio

Risers are very long pipes used to carry oil from the sea bed to offshore platforms floating on the water surface. Under the effect of sea currents, these flexible structures are especially susceptible to flow-induced vibrations, particularly since they have a relatively low mass compared to the mass of the displaced fluid. Generally, an offshore floating platform accommodates several riser pipes together with many other cylindrical structures. The interaction of these flexible structures can produce an even more complex problem, resulting in vibrations with rather unexpectedly higher amplitudes (Assi et al., 2010a). Flow interference from the platform hull, the soil on sea bed and the pipe itself can also increase the complexity of the flow, generating complex responses.

The riser may respond with different amplitudes and frequencies depending on the flow excitation and structural stiffness along the length of the pipe. Consequently, several modes of vibration with varying curvature appear along the span resulting in a very rich fluid–structure interaction mechanism (Srinil, 2010). In addition to that, flexible risers can be laid out in a catenary configuration which results in high curvature close to the region where it touches the bottom of the ocean, called the touchdown point.

In an attempt to understand and model the fluid-dynamic behaviour around curved sections of risers we have performed experiments with a curved, rigid circular cylinder in a water channel. This idealised experiment is far from reproducing the real conditions encountered in the ocean; nevertheless it should throw some light on understanding how the vortex shedding mechanism is affected by the curvature of the pipe. In addition to the phenomenological aspects, the present work may also serve as reference for validation and benchmarking of numerical simulations of fluid–structure interaction.

An investigation into the vortex shedding patterns and the fundamental wake topology of the flow past a stationary curved circular cylinder has been carried out by Miliou et al. (2007) and de Vecchi et al. (2008, 2009) based on computational fluid dynamics studies. As a result of pipe initial curvatures, flow visualisations highlight different kinds of wake characteristics depending on the pipe (convex or concave) configuration and its orientation with respect to (aligned with or normal to) the incoming flow. When the flow is uniform and normal to the curvature plane, the cross-flow wake dynamics of curved pipes behave qualitatively similar to those of straight pipes. This is in contrast to the case of flow being aligned with the curvature plane where wake dynamics change dramatically. However, these scenarios are pertinent to a particular stationary cylinder case in a very low-Reynolds number range. The VIV behaviour will further transform if the structure oscillates and interacts with the fluid wakes, depending on several fluid–structure parameters.

2. Experimental arrangement

Experiments have been carried out in the Circulating Water Channel of the NDF (Fluids and Dynamics Research Group) at the University of São Paulo, Brazil. The NDF-USP water channel has an open test section 0.7 m wide, 0.9 m deep and 7.5 m long. Good quality flow can be achieved up to 1.0 m/s with turbulence intensity less than 3%. This laboratory has been especially designed for experiments in flow-induced vibrations and more details about the facilities are described in Assi et al. (2006).

A rigid section of a curved circular cylinder, with an external diameter of $D=32$ mm, was made of ABS plastic and Perspex tubes according to the dimensions shown in Fig. 1. The curved cylinder was composed of a horizontal section with $10D$ in length, a curved section with a $10D$ radius and a vertical section with length h/D that could be varied with reference to the water line. The water level was set to 700 mm from the floor of the channel, which meant that the $10D$-long horizontal part of the cylinder was not close enough to the floor to suffer interference from the wall.

The model was connected by its upper end to a long pendulum rig (length $H=3.0$ m) that allowed the system to oscillate in two degrees of freedom (2-dof) in the cross-flow and streamwise directions. The model was attached to two pairs of coil springs that provided the stiffness of the system. The springs were set to provide the same natural frequency (f_0, measured in air) in both the cross-flow and streamwise directions. The design and construction of the pendular elastic rig was made by Freire and Meneghini (2010) based on a previous idea employed by Assi et al. (2009, 2010b) for experiments with VIV suppressors. The present apparatus has been validated for VIV experiments by Freire et al. (2009, 2011).

Two laser sensors measured the cross-flow and streamwise displacements of the pendulum referring to the displacement of the bottom tip of the models. A load cell was installed before the springs to allow for instantaneous measurements of lift and drag acting on the cylinder. (Hydrodynamic forces will not be discussed in this paper.) A particle-image velocimetry (PIV) system was employed to analyse the instantaneous wake patterns along the cylinder span.

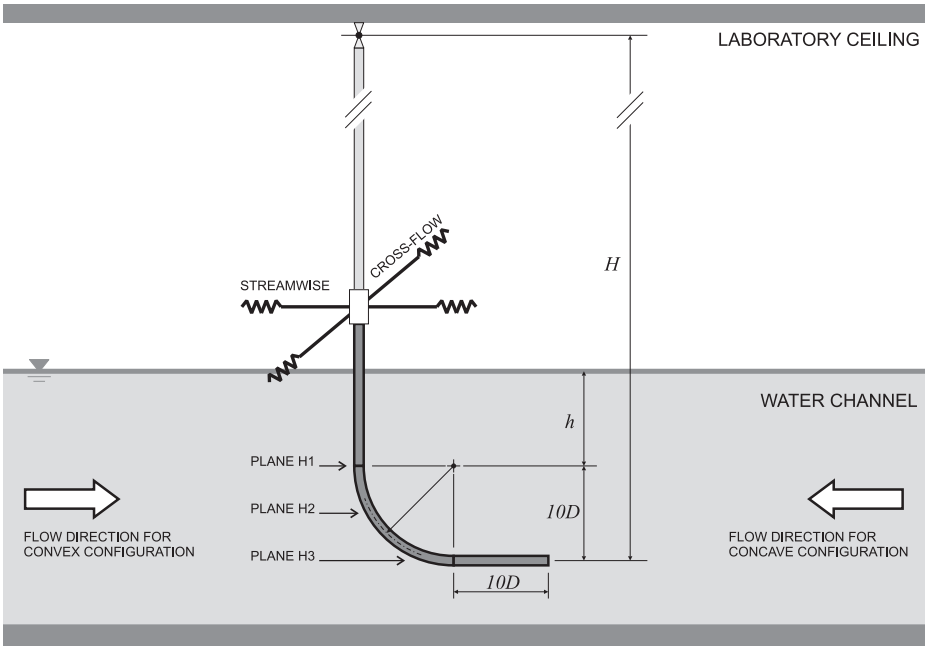

Fig. 1. Experimental arrangement in the NDF-USP circulating water channel. The cylinder was rotated by 180 degrees to arrange concave and convex configurations.

Table 1
Structural properties.

Model	m^*	ζ (%)	$m^*\zeta$
Straight cylinder	2.8	0.2	0.0056
Curved cylinders	2.1	0.2	0.0042

Regarding the flow direction, two orientations were investigated: a convex and a concave configuration according to the direction of the flow approaching the curvature. The flow direction in the test section of the water channel was not changed; naturally the curved cylinder was rotated by 180 degrees to allow for both concave and convex arrangements. This is also illustrated in Fig. 1.

Decay tests have been performed in air in order to determine the natural frequencies of the system in both directions as well as the level of structural damping. The apparatus with one universal joint and four springs turned out to present a very low structural damping of $\zeta = 0.2\%$, measured as a fraction of the critical damping. The total oscillating mass of the system was measured in air, resulting in a non-dimensional mass ratio m^*, defined as the ratio between the total mass and the mass of displaced fluid. Consequently, the mass-damping parameter $m^*\zeta$ of the system was kept to the lowest possible value in order to amplify the amplitude of response.

Table 1 presents a summary of the structural parameter for both the straight and curved cylinder.

3. Results for a straight cylinder

A preliminary VIV experiment was performed with a straight cylinder in order to validate the set-up and generate data for comparison. The same pendulum rig was employed, only replacing the curved model by a straight cylinder with the same diameter. This time, the straight cylinder was long enough to reach the bottom wall only leaving a 3 mm clearance to allow for free movement of the pendulum in any direction.

The dynamic response of the straight cylinder covered a reduced velocity range from 1.5 to 12, where reduced velocity (U/Df_0) is defined using the cylinder natural frequency of oscillation measured in air. The only flow variable changed during the course of the experiments was the flow velocity U, which, as for full-scale risers, alters both the reduced velocity and the Reynolds number between 750 and 15 000 for a maximum reduced velocity of 20.

The flow around a smooth, straight circular cylinder in the considered Reynolds number range (identified as sub-critical) is generally expected to be three-dimensional, with a laminar boundary layer over the cylinder surface and turbulent vortex wake. However, in the case of curved cylinder, the curvature plays a significant role in modifying the wake dynamics, which

depends on the leading geometry facing the approaching flow. This entails both the normal and axial flow components along the cylinder curved section, further complicating the spatio-temporal vortex shedding mechanisms, associated forces and frequencies. This has been exemplified by Miliou et al. (2007) for Re = 500.

Throughout the study, cylinder displacement amplitudes ($\hat{x}/D$ for the streamwise and $\hat{y}/D$ for the cross-flow directions) were found by measuring the root mean square value of response and multiplying by the square root of 2 (the so called harmonic amplitude). This is likely to give an underestimation of maximum response but was judged to be perfectly acceptable for assessing the general behaviour of VIV, since the response is mostly harmonic. Results presented in the present study correspond to the displacement of the lowest point of the model, i.e., the end of the cylinder closer to the section floor, thus representing the maximum displacement developed by each model. Consequently, the equivalent amplitude at the water surface for the cylinder with a 10D vertical section is 20% smaller than the amplitude indicated in the results. Applying similar corrections, amplitudes are 16% smaller for the cylinder with a 5D vertical section and 11% smaller for the cylinder with no vertical section.

Displacements are non-dimensionalised by the cylinder diameter D. The dataset for the straight cylinder is repeated in Figs. 2–5 to serve as reference.

Figs. 2 and 4 compare the reference cross-flow and streamwise responses obtained from two different runs with the straight cylinder. In the first one, the flow speed (U) was increased in 30 steps from zero to a maximum, while in the second it was decreased from the maximum to zero. Both data sets overlap rather well for all the reduced velocity range except for a region around $U/Df_0 = 6$ where the well-known phenomenon of hysteresis in the VIV response has been observed. The streamwise VIV response also seems to occur in two resonance ranges ($U/Df_0 = 2$ and 6), the so-called second and third instability ranges involving asymmetric vortices (Bearman, 1984).

Although the observed peak amplitude of $\hat{y}/D = 1.5$ around $U/Df_0 = 6$ is slightly higher than other results found in the literature for similar values of $m^*\zeta$ (for example, Assi et al., 2009) the general behaviour of both curves shows a typical response for 2-dof VIV. The higher amplitude found here could be explained by the very low mass-damping characteristics of the system and the geometric projection of the amplitude at the tip of the model and not at mid-length as usual.

Although the cylinder was initially aligned in the vertical position, in flowing water the mean drag displaces the cylinder from its original location reaching a slightly inclined configuration from the vertical. This was judged not to be detrimental to the experiment; hence the inclination of the cylinder was not corrected between each step. The same procedure was adopted for the curved cylinder.

Figs. 3 and 5 present the dominant frequency of response versus reduced velocity. Two dashed lines inclined with different slopes represent the region for a Strouhal number of 0.2 and 0.4, i.e., an estimation of the vortex shedding frequency for a straight cylinder in the cross-flow and streamwise direction respectively. It is clear that the straight cylinder

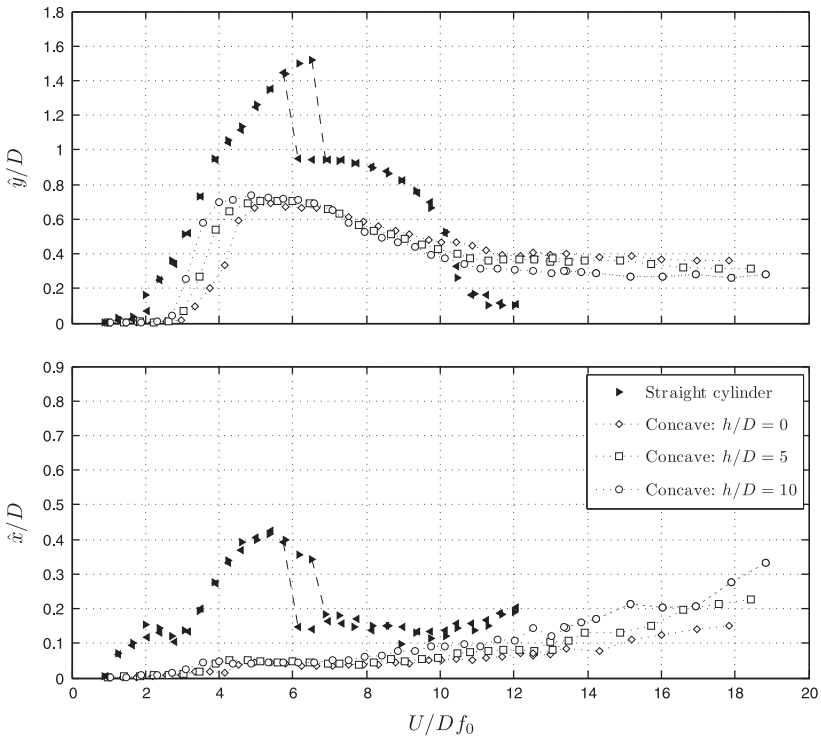

Fig. 2. Cross-flow ($\hat{y}/D$) and streamwise ($\hat{x}/D$) amplitude of vibration versus reduced velocity for a straight cylinder and concave configurations varying the vertical section length (h/D). Symbols ▸ are for runs with increasing flow speed, while ◂ are for decreasing.

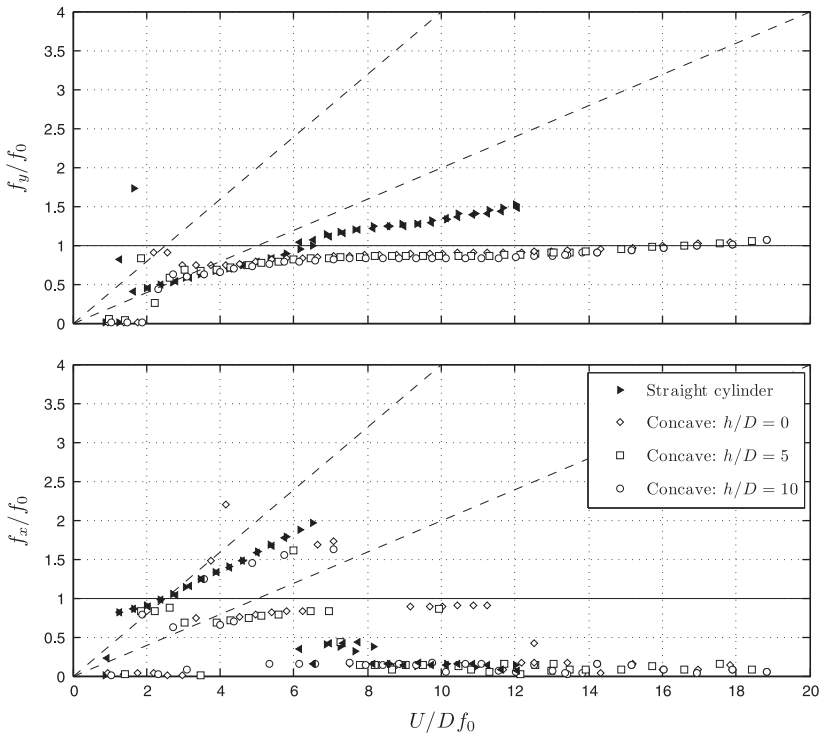

Fig. 3. Cross-flow ($\hat{y}/D$) and streamwise ($\hat{x}/D$) dominant frequency of response versus reduced velocity for a straight cylinder and curved concave configurations varying the vertical section length (h/D). Symbols ▸ are for runs with increasing flow speed, while ◂ are for decreasing.

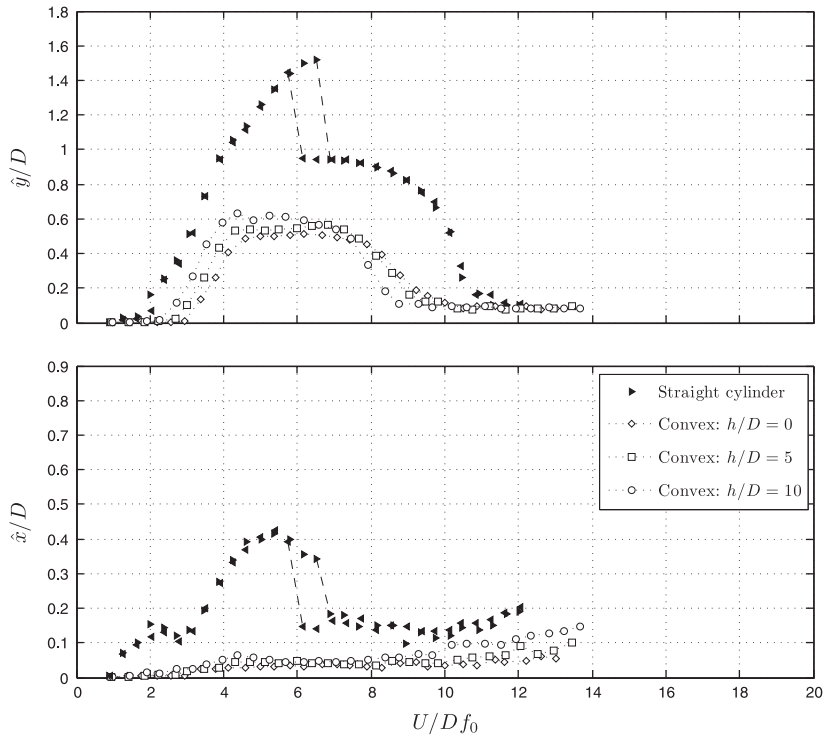

Fig. 4. Cross-flow ($\hat{y}/D$) and streamwise ($\hat{x}/D$) amplitude of vibration versus reduced velocity for a straight cylinder and convex configurations varying the vertical section length (h/D). Symbols ▸ are for runs with increasing flow speed, while ◂ are for decreasing.

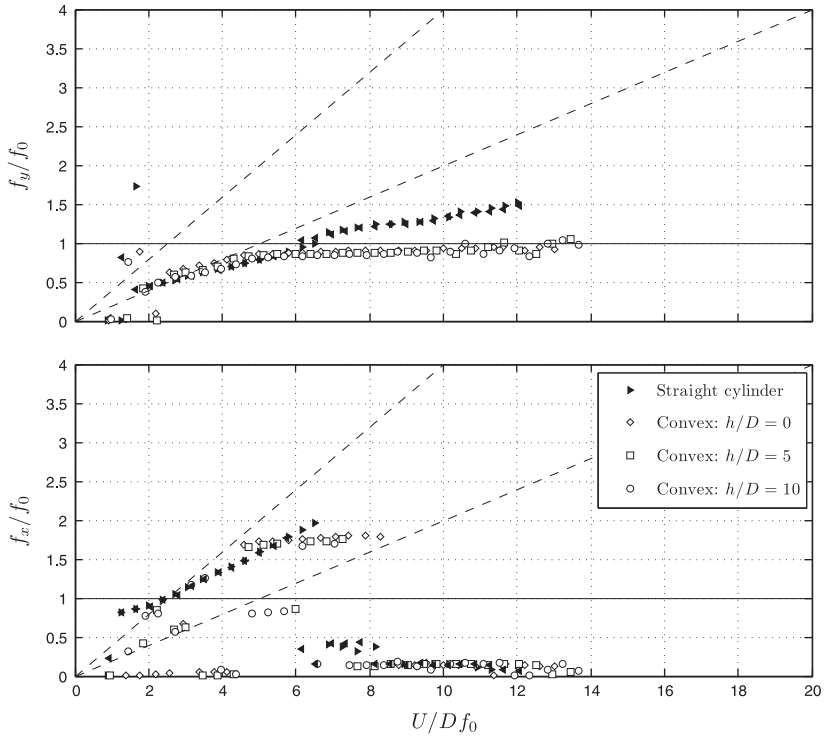

Fig. 5. Cross-flow ($\hat{y}/D$) and streamwise ($\hat{x}/D$) dominant frequency of response versus reduced velocity for a straight cylinder and curved convex configurations varying the vertical section length (h/D). Symbols ▸ are for runs with increasing flow speed, while ◂ are for decreasing.

presents a typical VIV response oscillating in the cross-flow direction with a frequency following the $\mathrm{St}=0.2$ line up to the beginning of the upper branch. Eventually, f_y/f_0 departs from $\mathrm{St}=0.2$ towards the unity value around $U/Df_0=6$. The behaviour observed for the streamwise vibration is also typical of VIV with the difference that the frequency of response is twice as that for the cross-flow direction during much of the synchronisation range.

4. Response of the curved cylinder

As mentioned above, experiments with the curved cylinder were performed taking into account two distinct configurations as far as the flow direction is concerned. In the concave configuration the flow approaches the model reaching first the horizontal section. As opposed to that, in the convex configuration the horizontal section is placed downstream of the curved and vertical parts.

4.1. Amplitude of vibration

In general terms, as presented in Figs. 2 and 4, the curved cylinders showed significantly less vibration for both concave and convex configurations when compared to the typical VIV response of the straight cylinder. Such a reduction is noticeable in both the cross-flow and streamwise responses. This clearly shows that the curvature of the cylinder modifies the vortex shedding mechanism in a manner that the structure extracts less energy from the flow. We shall return to this point when investigating the velocity flow field with PIV.

For each concave and convex configuration, the vertical section of the cylinder close to the free surface was varied in three different lengths: $h/D=0$, 5 and 10. The overall response for the three values of h/D is very similar, showing only minor differences at the beginning of the synchronisation range between $U/Df_0=3.0$ and 5.0. Apart from that, no distinct behaviour was observed as far as a variation in h/D is concerned for both concave and convex configurations.

The cross-flow displacement does not reveal distinct upper and lower branches of vibration such as those observed for a straight cylinder, but it produces a smooth curve that spans the whole synchronisation region with maximum amplitude around $\hat{y}/D=0.75$ for the concave and 0.65 for the convex configurations. No hysteresis is found.

However, the most interesting feature of such a behaviour is found when the convex response is compared to the concave one (Figs. 2 and 4). While the convex curve for $\hat{y}/D$ drops immediately between $U/Df_0=8$ and 10 to a level of $\hat{y}/D\approx 0.1$, the response for the concave case does not diminish, but is sustained for higher reduced velocities around $\hat{y}/D=0.3$ until the end of the experiment. Apparently there must be a fluid-elastic mechanism occurring for reduced

velocities above 8.0 for the concave configuration capable of extracting energy from the flow to sustain vibrations around $\hat{y}/D = 0.3$. We shall discuss this point later while analysing the PIV flow fields.

In the streamwise direction the responses of the curved cylinders are different from the typical VIV developed by the straight cylinder. Streamwise vibrations in the first and second resonance regions are totally suppressed, probably owing to the hydrodynamic damping effect induced by the cylinder's horizontal part. At the same time, the streamwise vibration $\hat{x}/D$ for the concave case also shows increasing amplitude beginning at reduced velocities higher than 10 and reaching $\hat{x}/D \approx 0.35$ for the highest flow speed. It coincides with the increased amplitude observed in the cross-flow direction and should be related to the same excitation mechanism. Once more, no distinct difference in the streamwise response was observed while varying h/D.

4.2. Frequency of vibration

Figs. 3 and 5 present the dominant frequency of oscillation non-dimensionalised by the natural frequency for both cross-flow and streamwise directions of motion. Results for the curved cylinder show a consistent behaviour in the cross-flow direction, with data points following the Strouhal line up to the upper branch peak but remaining closer to $f_y/f_0 = 1.0$ for the rest of the reduced velocity range. In the streamwise direction, we find data points following both Strouhal lines and also very low frequencies indicating random drifts instead of periodic oscillations. Since the displacements in the streamwise direction are much smaller for the curved cylinder than the straight one, we should expect broader frequency spectra dominating over the response.

One might remember that the straight and curved cylinder should have very similar values of added mass in the cross-flow direction, but slightly different values in the streamwise direction due to the geometric properties relative to the flow. We have not taken such effect into account in this paper, but it might be playing an important role defining the frequencies of oscillation in water.

4.3. Trajectories of motion

Fig. 6 qualitatively compares samples of displacement trajectories obtained for three experiments performed with the straight cylinder and the curved cylinders with $h/D = 10$. The straight cylinder presents distinct eight-shape figures typical of 2-dof VIV owing to the 2:1 ratio on the streamwise to cross-flow frequency of excitation. On the other hand, trajectories for both configurations of the curved cylinder reveal that the streamwise displacement is greatly reduced when compared to the straight cylinder. Both concave and convex cases show very little movement in the streamwise direction for the whole range of reduced velocity.

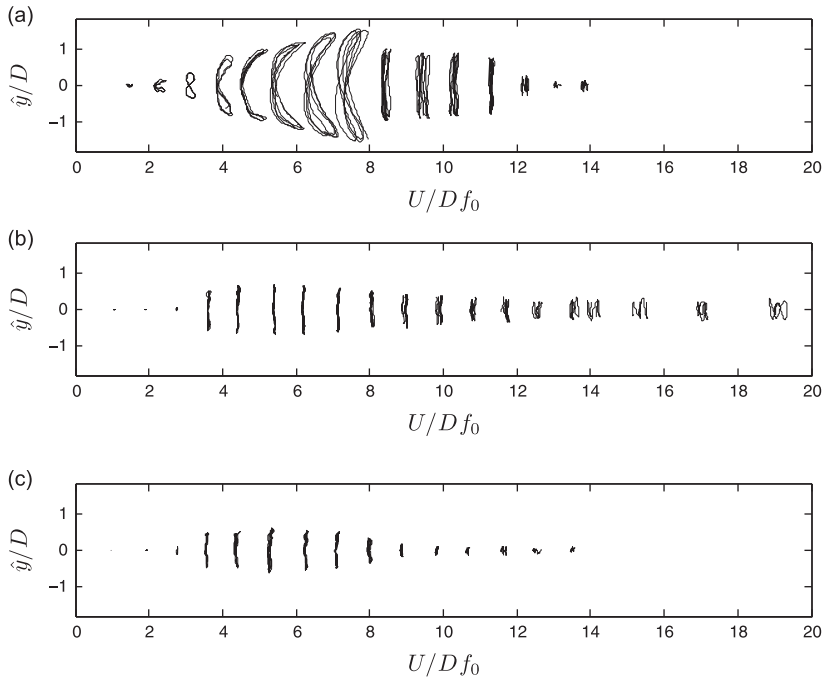

Fig. 6. Response trajectories of motion for a (a) straight cylinder and a curved cylinder in (b) concave and (c) convex configurations. Each trajectory was taken at the reduced velocity indicated in the horizontal axis. (a) Straight cylinder, (b) curved cylinder, concave configuration, $h/D = 10$, and (c) curved cylinder, convex configuration, $h/D = 10$.

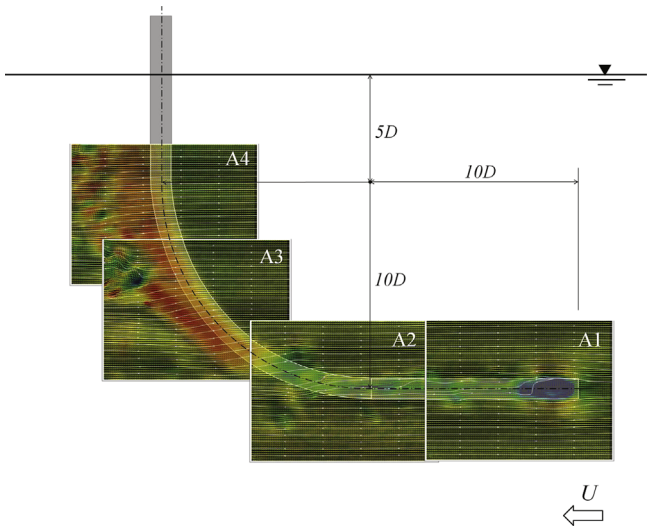

Fig. 7. Composition of instantaneous PIV velocity fields for concave configuration with $h/D = 5$.

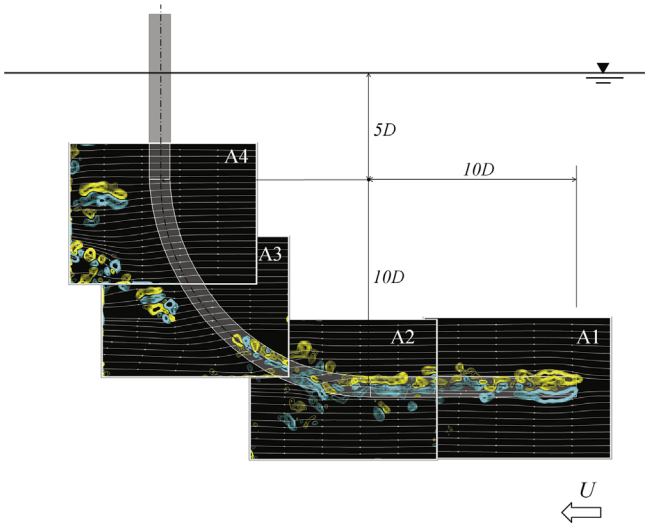

Fig. 8. Composition of instantaneous PIV vorticity fields for concave configuration with $h/D = 5$.

Another interesting observation relates to the movement of both curved cylinders. It is clear that for reduced velocities greater than 10 the convex cylinder shows small displacements in both directions, while vibrations are sustained until the end of the experiment for the concave case as shown in Figs. 2 and 4.

5. Velocity and vorticity fields of stationary cylinders

Two dimensional PIV (particle image velocimetry) measurements of the flow around the cylinder were performed, for both concave and convex configurations, on a vertical plane parallel to the plane of curvature. In addition, PIV measurements were also performed on three horizontal planes (marked H1, H2 and H3 in Fig. 1 across the cylinder diameter.

All PIV measurements were taken for $Re = 1000$ in the sub-critical Reynolds number regime found for a straight circular cylinder. According to Williamson (1996), the particular flow is in the shear-layer transition regime, characterised by an increase on the base suction, a gradual decrease in the Strouhal number and a decrease in the formation length of the mean recirculation region. These trends are caused by the developing instability of the separating shear layers from the sides of the body. The flow around a curved cylinder, which presents different elliptical cross-sections along the span, may behave slightly different from the above description. Further investigation is necessary in order to evaluate that.

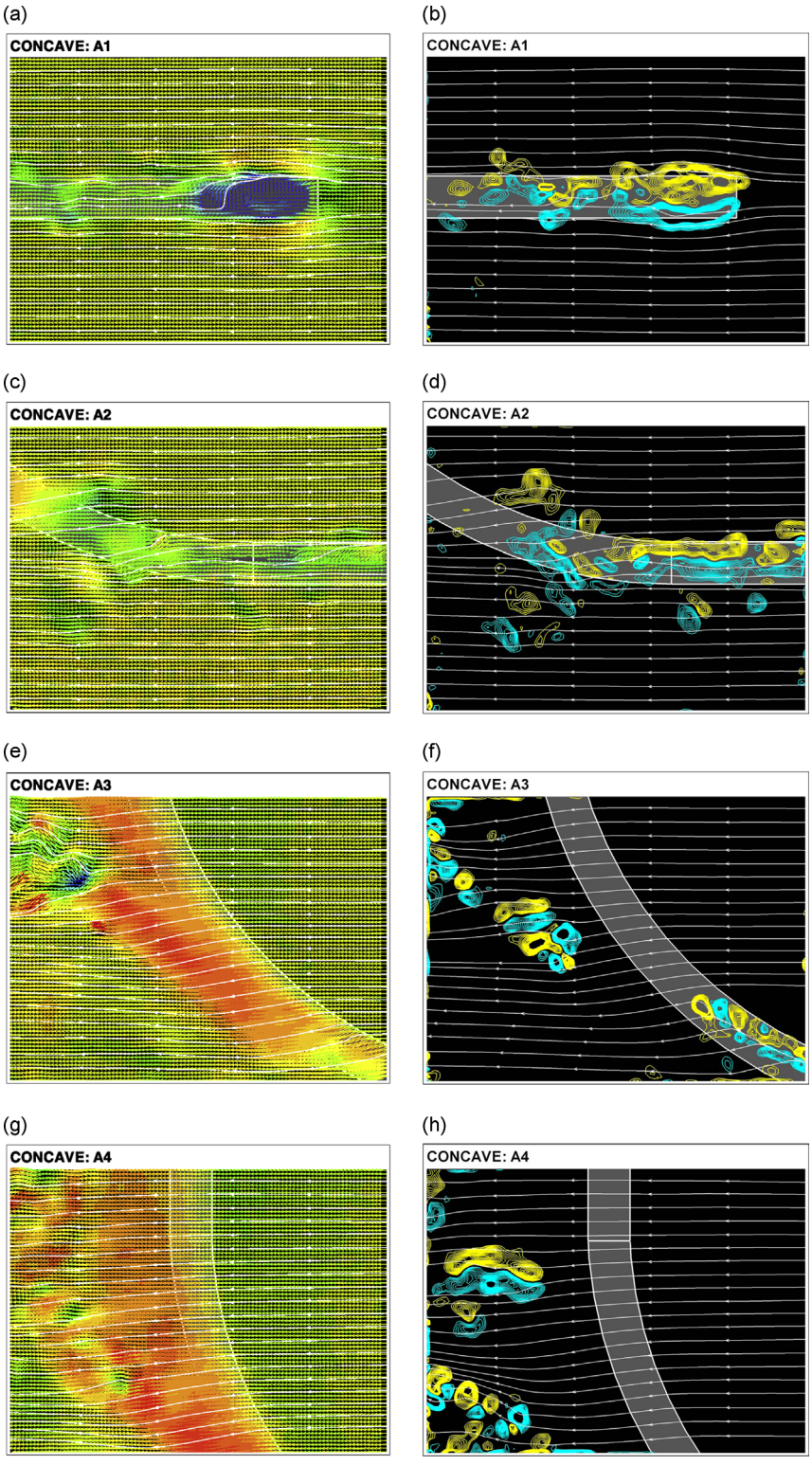

Fig. 9. Detailed velocity and vorticity fields from Figs. 7 and 8. Flow direction is from right to left. Re = 1000. Colour scale for velocity magnitude is from 0.004 m/s (blue) to 0.05 m/s (red). Colour scale for vorticity contours in the range $\pm 0{,}004\ s^{-1}$. (Velocity fields do not correspond to the vorticity fields in time.). (a) Velocity magnitude, A1, (b) vorticity contours, A1, (c) velocity magnitude, A2, (d) vorticity contours, A2, (e) velocity magnitude, A3, (f) vorticity contours, A3, (g) velocity magnitude, A4, and (h) vorticity contours, A4. (For interpretation of the references to color in this figure caption, the reader is referred to the web version of this article.)

5.1. Vertical plane

We shall start discussing the results obtained from the vertical plane, as presented in Figs. 7–12. Four visualisation areas for each configuration, labelled A1–A4, were conveniently distributed along the length of the cylinder in order to evaluate as much as possible to the flow pattern around the body. All four areas are in the same plane illuminated by the laser, which is parallel to the plane of curvature only dislocated by 1D from the centre of the cylinder towards the camera in order to capture the highest velocities induced by the vortex tubes. Figs. 9 and 12 show the location of each area composing the flow filed along the cylinder. It is important to note that each velocity field was obtained from a different acquisition instant; hence A1, A2, A3 and A4 are not correlated in time.

All PIV measurements were performed for a static cylinder at $\mathrm{Re} \approx 1000$. Of course the wake pattern for the static cylinder is expected to be different from the wake of an oscillating cylinder, but even an analysis of a fixed body can contribute to the understanding of the complex vortex–structure interaction occurring during the response. A similar approach was employed by Miliou et al. (2007) who performed numerical simulations for a static, curved cylinder between $\mathrm{Re} = 100$ and 500. The same colour scales have been employed from Figs. 7 to 12 to allow for direct comparison of velocity magnitude and vorticity contours.

With that in mind, let us analyse first the flow pattern around the concave configuration in Figs. 7–12. The overall flow around the body can be divided into two parts:

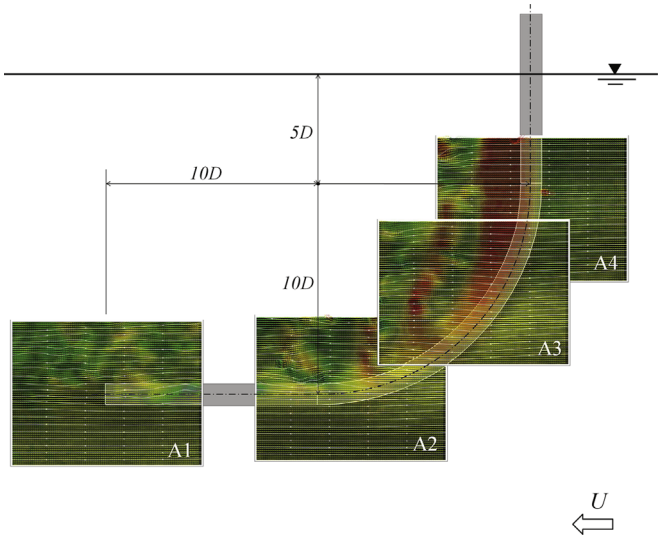

Fig. 10. Composition of instantaneous PIV velocity fields for convex configuration with $h/D = 5$.

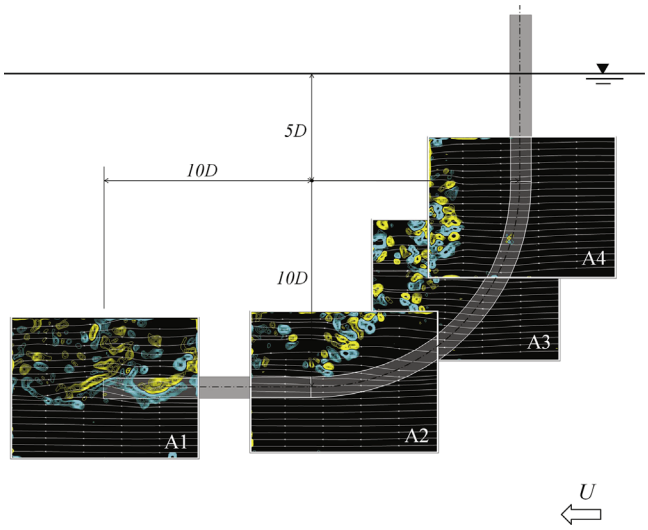

Fig. 11. Composition of instantaneous PIV vorticity fields for convex configuration with $h/D = 5$.

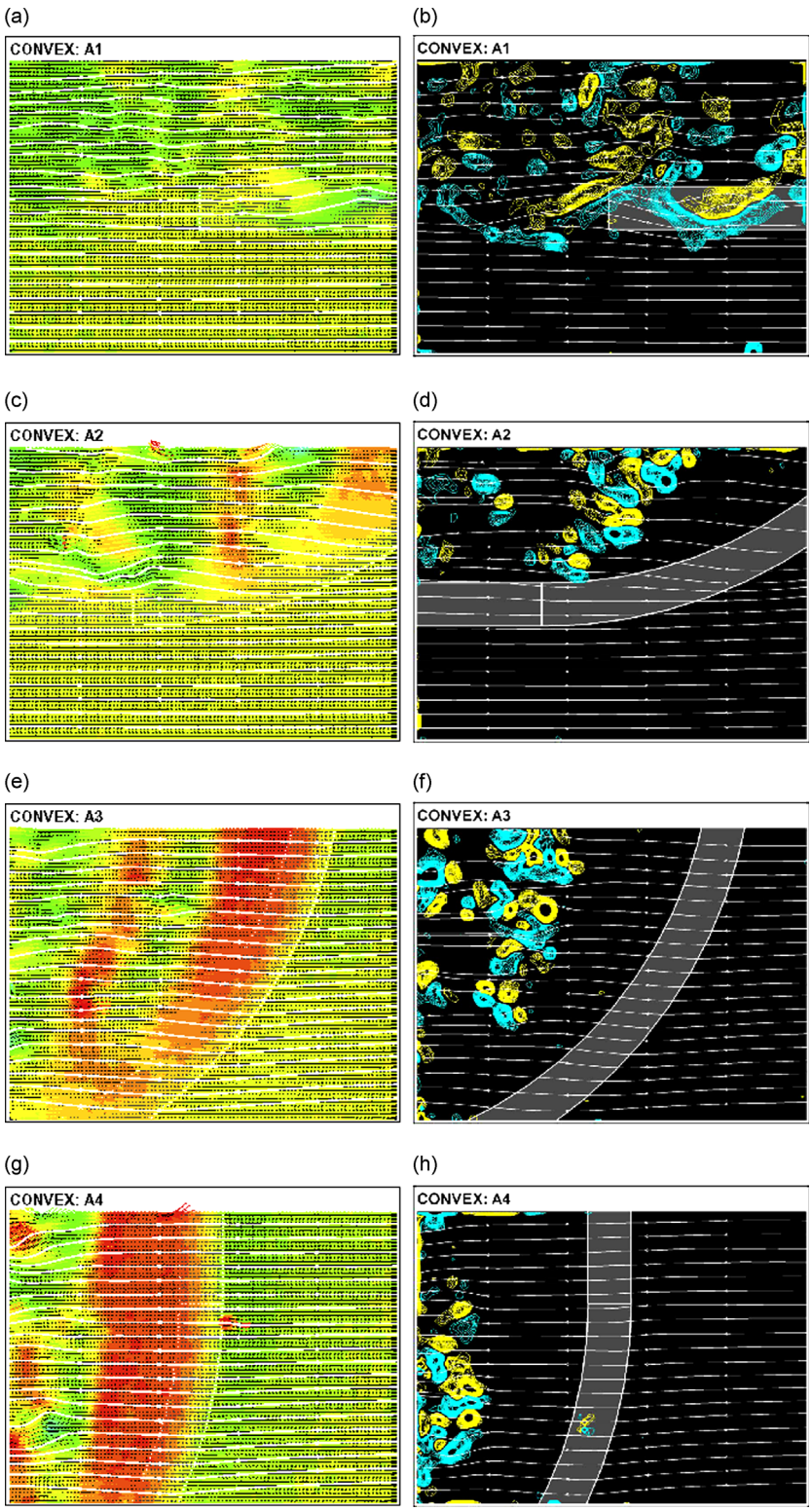

Fig. 12. Detailed velocity and vorticity fields from Figs. 10 and 11. Flow direction is from right to left. Re = 1000. Colour scale for velocity magnitude is from 0.004 m/s (blue) to 0.05 m/s (red). Colour scale for vorticity contours in the range $\pm 0.004\ s^{-1}$. (Velocity fields do not correspond to the vorticity fields in time.). (a) Velocity magnitude, A1, (b) vorticity contours, A1, (c) velocity magnitude, A2, (d) vorticity contours, A2, (e) velocity magnitude, A3, (f) vorticity contours, A3, (g) velocity magnitude, A4, and (h) vorticity contours, A4. (For interpretation of the references to color in this figure caption, the reader is referred to the web version of this article.)

(I) Areas A1 and A2 show the region where the flow is mostly parallel to the axis of the cylinder. Therefore, no clear vortex tubes are observed with concentrated axial vorticity. Instead, the flow along the horizontal length is disturbed by the separation occurring at the tip of the cylinder. Area A1 shows the flow approaching the disk facing upstream and separating into a recirculation bubble. The periodicity of the shedding associated with this region is also related to the flow speed and the diameter D, but no coherent vortices parallel to the cylinder are able to form. As a consequence, a cascade of small vortices is convected downstream along the horizontal length (see area A2) reaching the beginning of the curved section.

(II) Areas A3 and A4 show the region where the flow is mainly perpendicular to the axis of the cylinder. Coherent vortex tubes tend to form following the curvature of the body, but further downstream they are stretched and rapidly breakdown into smaller vortices that are convected by the flow. Area A3 shows the instant when a vortex tube is shed almost tangent to the curvature, while area A4, around the vertical section, reveal a formation region more or less aligned with the axis of the cylinder. Streamlines drawn in areas A3 and A4 reveal a non-negligible velocity component deflecting the flow downwards immediately after the vortex formation region. As we move along the cylinder towards the water line from A3 to A4 the downward component is gradually reduced until it eventually disappears towards the upper half of A4. This region marks the competition between two wake modes existent along the transition from curved to straight cylinder. This looks similar to Fig. 15 in Miliou et al. (2007), with $\mathrm{Re} = 100$, although without the cylinder horizontal section therein.

Analysing the flow pattern for the convex configuration in Figs. 10–12 we notice two striking differences:

Firstly, because the flow approaching the convex body does not encounter a blunt disk facing upstream, no strong separation or recirculation bubble is formed. As a consequence, the horizontal section seen in areas A1 and A2 is not exposed to a disturbed, unsteady flow parallel to the axis of the cylinder. In fact, A1 and A2 reveal that the upper half of the horizontal length is exposed to a periodic flow formed by a regular wake, while the bottom half experiences almost no perturbation, with streamlines showing a well behaved flow field parallel to the axis.

Secondly, looking at the upper half of the body (A3 and A4) we notice much stronger and coherent vortex tubes when compared to the flow around the concave configuration. Area A3 reveals some kind of vortex dislocation after a formation region that increases in length as we move upwards. Because the convex geometry does not encourage the vortex tubes to stretch and break, a periodic wake seems to be sustained farther downstream. In contrast with the flow around the concave configuration, the velocity field around the curved section has a non-negligible vertical component upwards. It is stronger in A2 and is gradually reduced as we move upwards along the curvature in A3. This looks similar to Fig. 3 in Miliou et al. (2007) for $\mathrm{Re} = 100$.

Gallardo et al. (2011) stated that there is a certain degree of alignment of the flow structures with the axial curvature of the cylinder, which tilts the flow structures with respect to the vertical direction. Fig. 12(e) and (f) captures this behaviour, also recognised in Fig. 2 of Gallardo et al. (2011) and Fig. 8 of Miliou et al. (2007).

5.2. Horizontal planes

Figs. 13 and 14 present PIV velocity fields for the three horizontal planes indicated by H1, H2 and H3 in Fig. 1. All measurements were performed with $h/D = 5$. Plane H1 was positioned at the transition from the straight to the curved section of the model, i.e., 5D below the water line. Plane H2 was located 5D below that position and plane H3 another 5D down towards the floor.

Fig. 13 presents results for the concave configuration. The two cameras were positioned underneath the model as viewing from the bottom through the glass floor. A light grey circle or ellipse marks the cross section of the cylinder at the illuminated plane. A dark grey rectangle represents the part of the curved model in front of the laser plane, while a dashed line illustrates the projection of the model behind the plane. Each image is composed of two PIV areas taken simultaneously; for some cases they overlap, for others they are apart.

In Fig. 13(a), for the horizontal plane at the transition from the straight to the curved section, we notice a wider wake with a longer formation region that generates stronger vortices. This formation is related to the strong vortex tubes parallel to the straight section presented in Fig. 9(g). Moving down to plane H2, the cross section of the cylinder turns into an ellipse. The wake becomes much narrower with a short formation length and no strong vortices are distinguishable in the downstream flow. Fig. 9(e) also showed that an oblique vortex tube would form closer to the cylinder with vortices breaking apart into smaller eddies. Farther down to plane H3, the cross section illuminated by the laser plane now shows the beginning of the horizontal portion of the model. No vortex wake is identified, but only a region of disturbed flow which agrees with pattern shown in Fig. 9(c).

Results for the convex configuration in Fig. 14 were obtained in the same way as the concave, the only difference being that the cameras were installed above the channel, viewing from the top through the free surface. As a consequence, plane H3 does not result in any useful velocity field once the flow that separates from the cylinder follows attached to the horizontal portion of the model, as seen in Fig. 12(c).

Fig. 14(a) presents velocity fields for the first plane H1 at the transition region. A rather wide wake with strong vortical structures is noticeable through high induced velocities. Again, the same pattern was captured on the vertical PIV shown in Fig. 12(g). Moving down to plane H2 we notice that an organised wake may still exist, even though the cross section of the cylinder turned into an ellipse. Vortex tubes were also verified to persist further downstream in Fig. 12(c) and (e) as

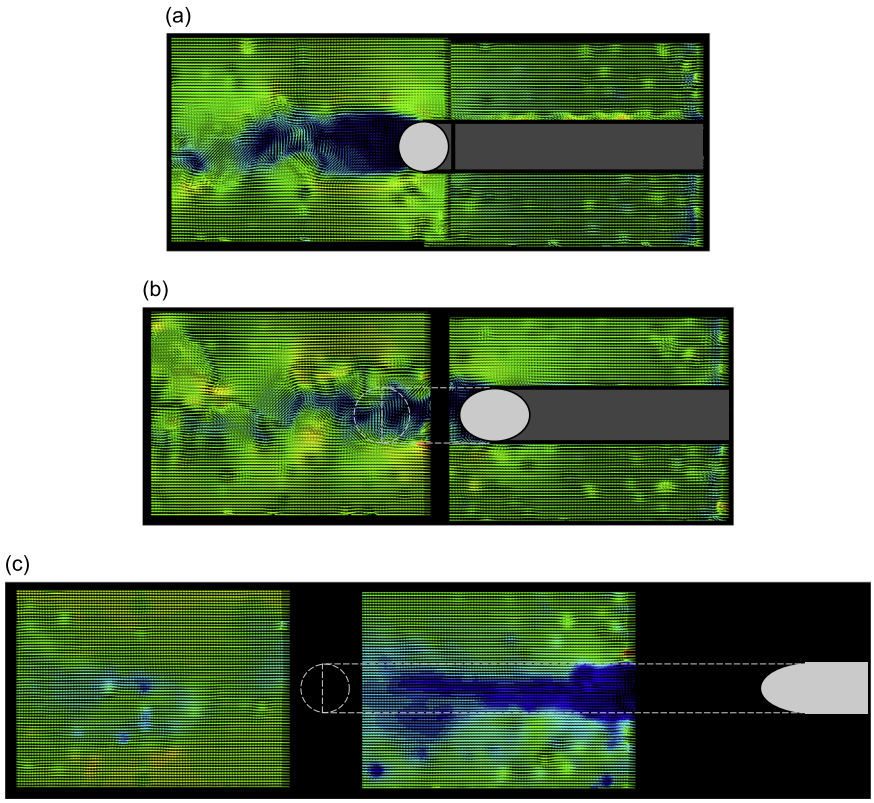

Fig. 13. Velocity fields for horizontal planes across the concave configuration. Refer to Fig. 1 for positions. Flow direction is from right to left. Re = 1000. Colour scale for velocity magnitude is from 0.004 m/s (blue) to 0.05 m/s (red). (a) Plane H1, (b) plane H2, and (c) plane H3. (For interpretation of the references to color in this figure caption, the reader is referred to the web version of this article.)

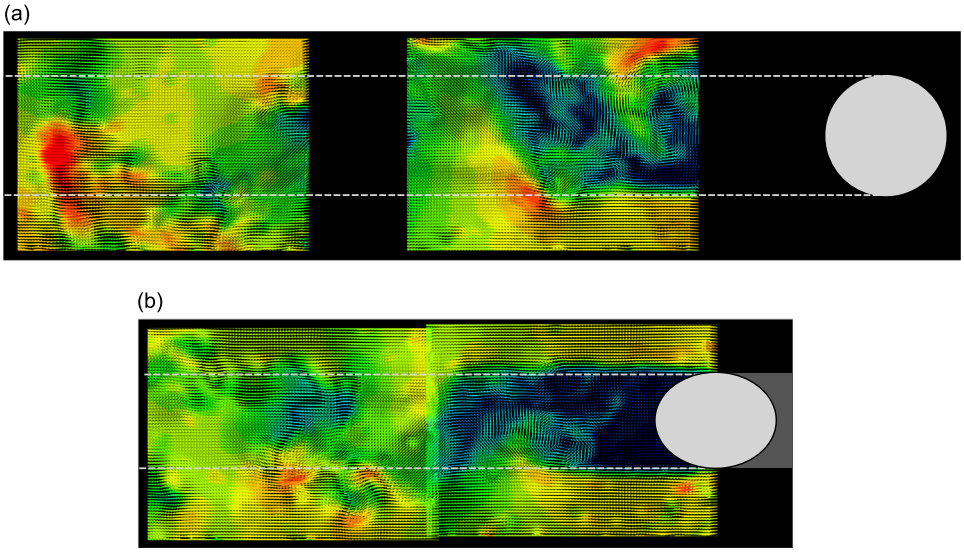

Fig. 14. Velocity fields for horizontal planes across the convex configuration. Refer to Fig. 1 for positions. Flow direction is from right to left. Re = 1000. Colour scale for velocity magnitude is from 0.004 m/s (blue) to 0.05 m/s (red). (a) Plane H1 and (b) plane H2. (For interpretation of the references to color in this figure caption, the reader is referred to the web version of this article.)

coherent flow structures appeared periodically downstream of the cylinder in the flow fields. Similar vortex structures were verified by Miliou et al. (2007) and Gallardo et al. (2011). This proves that the convex configuration is more prone to produce correlated vortex tubes along the curved length of the cylinder, while in the concave configuration vortices soon break apart as they are convected downstream.

Based on the results of Gallardo et al. (2011) for the convex configuration, one can observe that the interaction of the shear layers and thus the vortex formation length is a function of the cross-sectional shape being circular or elliptical, here represented by different planes along the cylinder span as can be seen in Fig. 14 and also in Fig. 3 of Gallardo et al. (2011).

Plane H1 in Fig. 14(a), which corresponds to plane $z/D = 16$ in Gallardo et al. (2011), shows that the shear layers interact in a farther downstream position from the body and the wake is wider compared to a horizontal position of the H2 plane in Fig. 14(b) where the cross-section of the cylinder is elliptical. In the latter case, seen also at the $z/D = 8$ plane in Gallardo et al. (2011), there are vortices produced within the recirculation region exhibiting the wavier shear layers.

6. The excitation mechanism

The main question to be answered by the present study is concerned with the fact that the amplitude in the cross-flow direction for the convex configuration is able to drop down to 0.1 for high reduced velocities while the concave configuration sustains vibration around 0.35. We believe this distinct behaviour between the convex and the concave configurations is related to the wake interference happening in the lower half of the cylinder due to perturbations generated in the horizontal section when it is positioned upstream.

In the concave configuration the horizontal part of the cylinder is located upstream of the curved and vertical parts. The approaching flow encounters a circular blunt leading edge with a clear separation region around the circumference (Fig. 9(a)). The flow that separates at the leading edge tends to create a separation bubble and latter reattaches along the horizontal section of the cylinder. Because the cylinder already presents cross-flow and streamwise vibrations, the three-dimensional separation bubble will not find a stable configuration nor a definite reattachment region, instead it will develop a periodic behaviour that may result in three-dimensional vortices being shed downstream, reaching the other parts of the cylinder. This is very clear in areas A1 and A2 of Figs. 7 and 9 for the static cylinder.

The fluid-elastic mechanism behind the response may be a composition of different phenomena acting at the same time. We believe this interaction between the disturbed flow from the upstream horizontal part with the curved and vertical parts is responsible for sustaining the level of vibration around $\hat{y}/D = 0.35$ and $\hat{x}/D = 0.35$. We suggest such an interaction may be occurring in the following forms:

(i) Vortices generated along the horizontal section may impinge on the curved part generating impulses in the same manner that large eddies of turbulence induce buffeting on elastic structures. Because the concave configuration has a longer section immersed in such a disturbed wake it is more susceptible to buffet. Evidence that a buffeting-like phenomenon might be occurring is that the streamwise vibration shows a considerable increase in amplitude with increasing flow speed further out of the synchronisation range. Fig. 6(b) also reveals that these vibrations are not harmonic and may even be chaotic, another evidence supporting the buffeting-excitation hypothesis.

(ii) The disturbed flow from the horizontal part may be disturbing and disrupting the vortex shedding mechanism from the curved and vertical sections, for example uncorrelating the vortex shedding mechanism in a curved region of the cylinder near the horizontal part. Also, the vortex wake along the curved-vertical half of the concave cylinder showed less correlation along the span, resulting in a lower peak of vibration during the synchronisation range.

(iii) Because the concave configuration has a fixed separation ring at the circle facing upstream, there might be some galloping-like instability related to the separation and reattachment of the three-dimensional bubble. This could generate non-resonant forces that could sustain some level of vibration for reduced velocities above the synchronisation range.

(iv) Finally, the concave configuration might experience some kind of instability related to the geometric arrangement of the experiment. Because the centre of pressure is located upstream of the vertical axis of the pendulum a minute deflection of the cylinder may result in a resolved force that will increase displacement. The opposite is true for the convex configuration in which the centre of pressure downstream of the vertical axis of the pendulum can only generate stabilising forces.

Of course all four mechanisms suggested above may also be occurring simultaneously or it may not even be possible to explain them separately. In addition, they might as well be very dependent on Reynolds number and amplitude of vibration.

7. Conclusions

We have experimentally investigated the two-degree-of-freedom VIV response of a rigid, curved circular cylinder with a low mass-damping ratio. With regard to the approaching flow (Reynolds number is in the range of 750–15 000) both concave and convex configurations were considered and the measured responses were compared with those of a typical straight cylinder. In summary, we conclude that:

(i) In general terms, a curved cylinder presents a lower peak of amplitude of vibration in both the cross-flow and streamwise direction when compared to a straight cylinder. Nevertheless, a considerable level of streamwise vibration, not attributed to VIV, was observed for reduced velocity as high as 18.

(ii) Although the peak amplitude is reduced, a curved cylinder may present a significant level of vibration that is sustained for higher values of reduced velocity beyond the end of the typical synchronisation range.
(iii) The concave configuration shows a considerable level of cross-flow vibration around $\hat{y}/d = 0.35$ up to the highest reduced velocity performed in this experiment.
(iv) The overall response showed little dependency on the vertical length immediately below the water line, at least for a section varying between $h/D = 0$ and 10.
(v) From the PIV study on a stationary curved cylinder, we suggest that the flow–structure interaction mechanism that differentiates the concave from the convex cylinder response may have its origin in the disturbed flow that separates from the horizontal part located upstream. This could be related to buffeting, galloping, disturbed VIV or geometric instabilities.

Future work should concentrate on correlated PIV analyses of the vortex formation along the curvature as well as on measurements of the flow field on planes perpendicular to the plane of curvature. An investigation of the interference effect generated by the separation at the tip of the horizontal section could also help towards understanding the response. PIV and instantaneous force measurements for an oscillating cylinder, especially at high reduced velocities, could throw some light into the actual mechanism of excitation.

Acknowledgements

G.R.S. Assi wishes to acknowledge the support of CNPq (308916/2012-3) and FAPESP (11/00205-6). C.M. Freire acknowledges support from FAPESP (10/00053-9). N. Srinil is grateful to the “Sir David Anderson Award” from the University of Strathclyde and the “Early Career Researcher International Exchange Award” supported by The Scottish Funding Council.

References

Assi, G.R.S., Meneghini, J.R., Aranha, J.A.P., Bearman, P.W., Casaprima, E., 2006. Experimental investigation of flow-induced vibration interference between two circular cylinders. Journal of Fluids and Structures 22, 819–827.
Assi, G.R.S., Bearman, P.W., Kitney, N., 2009. Low drag solutions for suppressing vortex-induced vibration of circular cylinders. Journal of Fluids and Structures 25, 1–10.
Assi, G.R.S., Bearman, P.W., Meneghini, J.R., 2010a. On the wake-induced vibration of tandem circular cylinders: the vortex interaction excitation mechanism. Journal of Fluid Mechanics 661, 365–401.
Assi, G.R.S., Bearman, P.W., Kitney, N., Tognarelli, M.A., 2010b. Suppression of wake-induced vibration of tandem cylinders with free-to-rotate control plates. Journal of Fluids and Structures 26, 1045–1057.
Bearman, P.W., 1984. Vortex shedding from oscillating bluff bodies. Annual Review of Fluid Mechanics 16, 195–222.
Freire, C.M., Korkischko, I., Meneghini, J.R., 2009. Development of an elastic base with tow degrees of freedom for VIV studies. In: Proceedings of COBEM 2009 – 20th International Congress of Mechanical Engineering, 2009, Gramado, Brazil.
Freire, C.M., Meneghini, J.R., 2010. Experimental investigation of VIV on a circular cylinder mounted on an articulated elastic base with two degrees-of-freedom. In: Proceedings of BBVIV6 – IUTAM Symposium on Bluff Body Wakes and Vortex-Induced Vibrations, 2010, Capri, Italy.
Freire, C.M., Korkischko, I., Meneghini, J.R., 2011. Defining a parameter of effectiveness for the suppression of vortex-induced vibration. In: Proceedings of OMAE2011 – 30th International Conference on Ocean, Offshore and Arctic Engineering, 2011, Rotterdam, The Netherlands.
Gallardo, J.P., Pettersen, B., Andersson, H.I., 2011. Dynamics in the turbulent wake of a curved circular cylinder. Journal of Physics: Conference Series 318, 062008.
Miliou, A., De Vecchi, A., Sherwin, S.J., Graham, M.R., 2007. Wake dynamics of external flow past a curved circular cylinder with the free stream aligned with the plane of curvature. Journal of Fluid Mechanics 592, 89–115.
Srinil, N., 2010. Multi-mode interactions in vortex-induced vibrations of flexible curved/straight structures with geometric nonlinearities. Journal of Fluids and Structures 26, 1098–1122.
de Vecchi, A., Sherwin, S.J., Graham, J.M.R., 2008. Wake dynamics of external flow past a curved circular cylinder with the free-stream aligned to the plane of curvature. Journal of Fluids and Structures 24, 1262–1270.
de Vecchi, A., Sherwin, S.J., Graham, J.M.R., 2009. Wake dynamics past a curved body of circular cross-section under forced cross-flow vibration. Journal of Fluids and Structures 25, 721–730.
Williamson, C.H.K., 1996. Vortex dynamics in the cylinder wake. Annual Review of Fluid Mechanics 28, 477–539.